

Geophysical Research Letters®

RESEARCH LETTER

10.1029/2021GL095739

Key Points:

- The criterion of an electrical resistance jump is sensitive to detect 1%–2% melt fraction of bulk iron to 135 GPa in diamond anvil cells
- The slopes in the temperature-resistance profile are changed across the solid-solid and slow-fast recrystallization transitions of iron
- The melting temperature of iron is ~4306 K at core-mantle boundary pressure, consistent with latest static and shockwave experiments

Supporting Information:

Supporting Information may be found in the online version of this article.

Correspondence to:

J. Liu,
jinliuyc@foxmail.com





Citation:

Hou, M., Liu, J., Zhang, Y., Du, X., Dong, H., Yan, L., et al. (2021). Melting of iron explored by electrical resistance jump up to 135 GPa. *Geophysical Research Letters*, 48, e2021GL095739. <https://doi.org/10.1029/2021GL095739>

Received 19 AUG 2021

Accepted 8 OCT 2021

Melting of Iron Explored by Electrical Resistance Jump up to 135 GPa

Mingqiang Hou^{1,2}, Jin Liu^{2,3,4} , Youjun Zhang⁵ , Xueyan Du² , Hongliang Dong², Limin Yan² , Junyue Wang², Lin Wang⁶, and Bin Chen²

¹State Key Laboratory of Geodesy and Earth's Dynamics, Innovation Academy for Precision Measurement Science and Technology, Chinese Academy of Sciences, Wuhan, China, ²Center for High Pressure Science and Technology Advanced Research, Shanghai, China, ³State Key Laboratory of Geological Processes and Mineral Resources, China University of Geosciences, Wuhan, China, ⁴CAS Center for Excellence in Deep Earth Science, Guangzhou, China, ⁵Institute of Atomic and Molecular Physics, Sichuan University, Chengdu, China, ⁶Center for High Pressure Science (CHiPS), State Key Laboratory of Metastable Materials Science and Technology, Yanshan University, Qinhuangdao, China

Abstract The melting temperature (T_m) of iron at megabar pressures constrains the Earth's core temperature structure and dynamics. Previous experimental studies demonstrated large discrepancies in T_m at high pressures. We used the intrinsic resistance discontinuity across solid-liquid transition as a melting criterion to study the melting behavior of iron in laser-heated diamond anvil cells. The resistance jump is sensitive to the incipient melting, capable of detecting the emergence of less than 2 vol.% melts. We found a high melting curve of iron at 30–135 GPa, but a relatively low-transition temperature of the slow-fast recrystallization. The determined T_m of iron is 4306(±300) K at the core-mantle boundary (CMB) pressure in good agreement with the static and shockwave experimental results by Anzellini et al. (2013, <https://doi.org/10.1126/science.1233514>) and Li et al. (2020, <https://doi.org/10.1029/2020gl087758>). The high melting point of iron implies a high and steep geothermal gradient and influences a heat flow across the CMB.

Plain Language Summary The melting of iron is fundamental to constrain the thermal structure, solidification, heat flux, and evolution of the Earth's core. Here, we propose a sensitive melting criterion, the resistance discontinuity across the phase transition, which is capable of detecting 2 vol.% melting of the bulk sample. Using this criterion, we determined the melting temperature of iron up to 135 GPa. The new melting curve of iron reconciles with the most recent shockwave and static experimental results, indicating a melting temperature of 4306(±300) K at the Earth's core-mantle boundary. Large discrepancies existing in the melting of iron are unlikely caused by varying melting criteria, while chromatic aberrations should be one of the major reasons resulting from refractive optical lens in the temperature measurement system.

1. Introduction

The solid inner core of the Earth is growing out of the liquid outer core, primarily composed of iron with 5%–10% nickel and a small number of light elements (Hirose et al., 2013). The inner core is expected to contain fewer light elements as they prefer staying in the liquid outer core. Those elements have a great influence on the melting behavior of iron (e.g., Liu et al., 2016; Morard et al., 2008, 2017). In general, the incorporation of light elements such as oxygen, silicon, and sulfur could depress the melting point of iron by up to 700 K at the inner core boundary (ICB) (Alfè et al., 2002). It is thus expected that the upper bound of the temperature at the ICB is the melting point (T_m) of iron at 330 GPa, while the lower bound depends on the identity and concentration of light elements. That is, the T_m values of iron and iron alloys at high pressure present the key to decode the temperature distribution of the Earth's core as well as the evolution and dynamics related to this region, including heat budget and the generation of magnetic field, heat flow across the ICB and the core-mantle boundary (CMB), and the crystal structure and density deficit of the inner core (Fei et al., 2016; Vočadlo et al., 1999).

Extensive studies have been dedicated to constrain the T_m of highly compressed iron including dynamic and static high-pressure experiments (e.g., Aquilanti et al., 2015; Brown & McQueen, 1986; Nguyen &

Holmes, 2004; Shen et al., 1998; Sinmyo et al., 2019; Turneure et al., 2020; Williams et al., 1991; Yoo et al., 1993) and theoretical calculations (e.g., Alfè et al., 2002; Vočadlo et al., 2003). However, it has led to an unacceptable discrepancy in the estimates of the temperature distribution in the center of our planet. Previous studies reported a range of T_m values of iron from 4850 to 7600 K extrapolated to the ICB pressure (Boehler, 1993; Williams et al., 1987). Such a large discrepancy calls for efforts to further constrain the T_m values of iron at high pressure by combining multiple techniques.

A battery of methods has been employed to determine the onset of melting such as fluid flow, quench texture, the relationship between temperature and laser power, optical reflectivity, diffuse scattering in synchrotron X-ray diffraction (XRD) patterns, synchrotron Mössbauer spectroscopy, and X-ray absorption spectroscopy (Anzellini et al., 2013; Aquilanti et al., 2015; Boehler, 1993; Jackson et al., 2013; Murphy et al., 2011; Nguyen & Holmes, 2004; Shen et al., 1998; Sinmyo et al., 2019; Williams et al., 1991; Zhang et al., 2016). It is worth noting that these melting criteria have different sensitivities to incipient melting. For instance, those X-ray-based methods can definitely identify the presence of melt in the sample chamber, but it generally requires a large fraction of melt as well as sufficient thickness in the restricted probing area. Due to a runaway melt from the laser spot, the determined temperature values might differ from the T_m at high pressure. On the contrary, the use of electrical resistance as a melting criterion may overcome these limitations, since electrical resistance reflects the change in the bulk sample, instead of a particular probed area. More importantly, a thick sample of $>4\text{--}5\text{ }\mu\text{m}$ is not a prerequisite to maintain data quality of electrical resistance measurements and thus it has the capability to extend such measurements to multimegabar pressures (Anzellini et al., 2013).

Furthermore, electrical resistance discontinuity of iron in an internal resistive heating system was proved to be a good criterion of determining phase boundary in early diamond-anvil cell (DAC) experiments by Boehler (1986), Liu and Bassett (1975), and Mao et al. (1987). Sharp changes in the electrical resistivity of iron have been observed at the onset of melting at high pressure by large volume press experiments (e.g., Deng et al., 2013; Silber et al., 2018; Yong et al., 2019). Recently, Basu et al. (2020) and Sinmyo et al. (2019) used voltage discontinuity in an internal resistive heating DAC and resistance discontinuity in a laser-heating DAC to determine the T_m of iron at high pressures. However, a difference of about 400 K has been reported in the T_m value of iron at 51 GPa among Basu et al. (2020), Ohta et al. (2016), and Sinmyo et al. (2019). At the CMB pressure, the difference becomes greater than 1000 K. The discrepancies may be ascribed to the following factors. First, as a common consensus, the temperature would mostly keep constant at the melting point because of latent heat. The electrical resistance of a metal would further increase with increasing melt fraction. However, both the temperature and resistance values of iron continue increasing after the determined melting point at 31–84 GPa in Basu et al. (2020), suggesting that melting temperatures could have been underestimated. Second, we observed severe deformation of the sample on approach to the onset of melting when both sizes of the sample were simultaneously and homogeneously heated in the resistivity measurements of iron and iron-rich alloys (Zhang et al., 2020, 2021). The severe deformation would significantly lower the sensitivity of the electrical resistance jump as a criterion in determining the high-pressure melting of iron in DACs. The “resistance jump” observed in Basu et al. (2020) could be caused by the sample deformation prior to melting; accordingly, the monotonic increase in the temperature-resistance relation at temperatures greater than their reported melting point can be explained. Lastly, homogeneous resistive or laser heating of the sample could depress the sensitivity of the electrical resistance discontinuity across the solid phase transitions of iron. This could be the reason why no solid phase transition was identified in Sinmyo et al. (2019) and no slow-fast recrystallization was observed in Basu et al. (2020) by using resistance discontinuity.

We have developed a new methodology to accurately identify the resistance discontinuity in DAC experiments on iron melting up to 135 GPa following the preliminary results of Hou (2016). The electrical resistance jump is used to determine the T_m of iron at high pressure in accordance with the phase relation of iron in this study. Here, we improve the sensitivity of the electrical resistance discontinuity as a criterion in determining phase transitions. At the same time, the other three melting criteria are coupled to cross-check, that is, the temperature-laser power relation, quench texture, and fluid flow. Our results show a high melting profile of iron at 30–135 GPa, which is in consonance with the synchrotron-based fast XRD study by

Anzellini et al. (2013) and the latest shock experiments by Li et al. (2020). Our study supports the warmer interiors of rocky planets including Earth, Mercury, and Mars.

2. Experiment

Symmetric DACs with beveled (300/150 μm) and flat diamond anvils (300 μm) were employed to generate high pressure. A hole of 4/5 culet size was drilled by laser ablation in a pre-indented Re gasket. Cubic boron nitride (c-BN) was packed into the hole, serving as an inner gasket and electrical insulation. A hole of 80 μm in diameter was drilled in the center of c-BN inner gasket. High-purity iron (99.9%) sample was purchased from Alfa Aesar Company and used as starting materials. A strip with ~ 40 μm in width and ~ 8 μm in thickness was cut from a pre-compressed thin Fe foil and placed into the sample chamber, where the iron strip was in contact with two Pt electrodes (Figure S1 in Supporting Information S1). This assembly is a standard two-terminal method. Fused silica was used as both pressure medium and thermal insulation, which was preheated at 1473 K for 10 h to remove moisture. All pressures were determined by Raman spectra of diamond anvil tips after laser heating (referred as P_0). Thermal pressures were estimated according to Fei et al. (2016) and Dorogokupets et al. (2017) for hcp-Fe and fcc-Fe, respectively. The pressure at high temperature (referred as P_T) was corrected by adding half of the calculated thermal pressures in the exact same way by Aquilanti et al. (2015) and Zhang et al. (2016). The uncertainty in the pressure is within 3 GPa determined by using this method according to our previous X-ray diffraction studies on iron, in which the similar experimental assembly was employed (Zhang et al., 2020) (Figure S2 in Supporting Information S1).

An ytterbium CW fiber laser with a wavelength 1,070 nm was employed for heating up one side of the sample. The laser spot was about 30 μm in the full width at half maximum focused on the sample position. Acton SP-2156 spectrograph was equipped with PIXIS-256BR CCD camera and they were used to collect spectra emitting from the hot spot of the sample. The temperature measurement system was calibrated at 2993 K using an Oriel NIST traceable calibrated quartz tungsten halogen lamp. Temperature was determined by fitting the spectrum between 600 and 750 nm with Planck radiation function. The uncertainties are ~ 150 and ~ 300 K at temperatures of <4000 K and >4000 K, respectively.

Electrical resistance of the sample assembly was measured at a constant current (10 mA) by using a high precession source meter (Keithley-2410). The electrical resistance was recorded when temperature measurements were collected. We normalized the electrical resistance (R) at high temperature by an initial electrical resistance (R_0) at 300 K to obtain uniform $T-R/R_0$ relations. The T_m value was determined at the onset of a sudden electrical resistance increase in the $T-R/R_0$ relation, while the gradual slope change of $T-R/R_0$ was assigned to the solid-solid phase transition of iron at pressures below 100 GPa. Five sets of experiments were conducted in the present work (Table S1 in Supporting Information S1). Diamond anvils with culet size of 300 μm were used to perform experiment M1 (20.2, 35.3, 49.5, 51.5, and 56.0 GPa). Experiments M2 (56.5 and 74.8 GPa), M3 (77.5 and 110.0 GPa), M4 (30.0, 35.7, and 48 GPa), and M5 (68.0, 116.0, 109.0, and 97.0 GPa) were performed by using the beveled diamond anvils with the culet size of 300/150 μm . We note that the sample size is key to guaranteeing the high sensitivity of electrical resistance discontinuity in determining the phase transitions of iron at high pressure. The sample should be about twice as wide as the homogeneous laser heating spot in order to minimize the deformation of the sample at high temperature, because the center ~ 10 μm would be homogeneously heated for a 20–30 μm laser spot. Additionally, the electrical current used to probe the resistance of the sample should be small enough to avoid any significant resistive heating. These considerations assure a more precise determination of the phase diagram of iron at high P - T over previous methods using electrical resistance to monitor phase transitions of iron.

3. Results

3.1. The Consistence Among Melting Criteria

Representative $T-R/R_0$ relations at 30.0 and 110.0 GPa are shown in Figure 1. The electrical resistance of iron monotonically increases as a function of temperature. At $P_0 = 30.0$ GPa, the two obvious slope changes could be observed. The first one was located at ~ 2170 K, which is in good accordance with the hcp-fcc phase boundary of iron (e.g., Shen et al., 1998). Consequently, this temperature value was denoted as the phase boundary of the hcp-fcc transition at 35.7 GPa. At ~ 2800 K, the temperature almost remained constant with

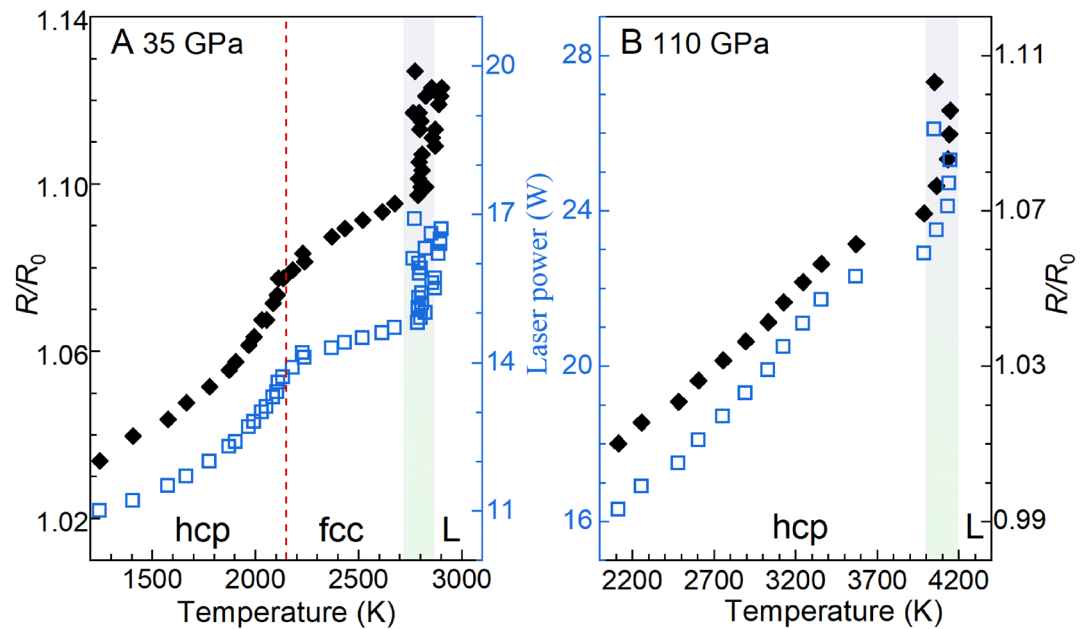


Figure 1. The R/R_0 ratio and laser power as a function of temperature at (a) 35 GPa and (b) 110 GPa after heating. R_0 and R values are electrical resistances at room and high temperatures, respectively. Blue and black symbols represent the data of R/R_0 and laser power, respectively.

increasing laser power, whereas the electrical resistance still climbed up. This is, electrical resistance jump occurred at this temperature, associated with the higher resistance of melt compared with that of the solid phase and the increasing volume of the melt. We note that new solid iron surface could be exposed because of the outward flow of liquid iron when the measured temperature dropped to 2704 K. Up further laser heating, it increased to 2904 K. This phenomenon was in general caused by fluid flow that could be visually observed on the sample surface when being monitored by a high-resolution camera (Boehler, 1993). When fluid flow occurred, the new solid surface would be directly exposed to the laser beam, likely resulting in a significant drop in temperature. However, the solid would quickly melt upon further heating and the temperature could reapproach the T_m . At $P_0 = 110.0$ GPa, the electrical resistance of iron increases monotonically without a slope change observed prior to melting, indicating that iron was staying in the hcp phase. At the same time, fluid flow was observed as the temperature suddenly dropped approximately from 4150 to 4050 K upon melting.

As a comparison, temperature-laser power (T -Power) relations of our experiments are shown in Figure 1. The variations in the T -Power relations are similar to the T - R/R_0 upon laser heating. The consistence between the T -Power and T - R/R_0 relations was reached when confirming the hcp-fcc phase transition of iron at 35 GPa. As mentioned above, fluid flow was observed during melting. Fluid flow can significantly change the surface morphology of the sample. The quench texture could be evidently observed in the center of the laser-heated spot (Figure 2). A flocculent texture in the melting area is distinguished from the unmelted crystal surface. The cross sections of the heated sample were prepared by focused ion beam (FIB) milling, allowing to observe the distribution of grain size inside. The melting layer was ~ 1.0 μm in thickness on the surface of the sample directly exposed to the laser beam. By contrast, the grain morphology of the unmelted area exhibited a distinguishable appearance with pin-like grains of 0.4 μm in horizontal direction and at least 2.5 μm in vertical direction.

Electrical resistance jump is a melting criterion sensitive to determine the onset of melting of iron. The laser spot focus on the sample was about 30 μm in diameter but the melting area was about 8 μm (Figure 2). A thickness of ~ 1 μm was observed for the melting layer that is a small fraction of the sample directly subjected to laser heating. In other words, the total melting portion is less than 2 vol.%, suggesting that the criterion of electrical resistance jump could distinguish the partial melting of 1–2 vol.% in the bulk sample. It is worth

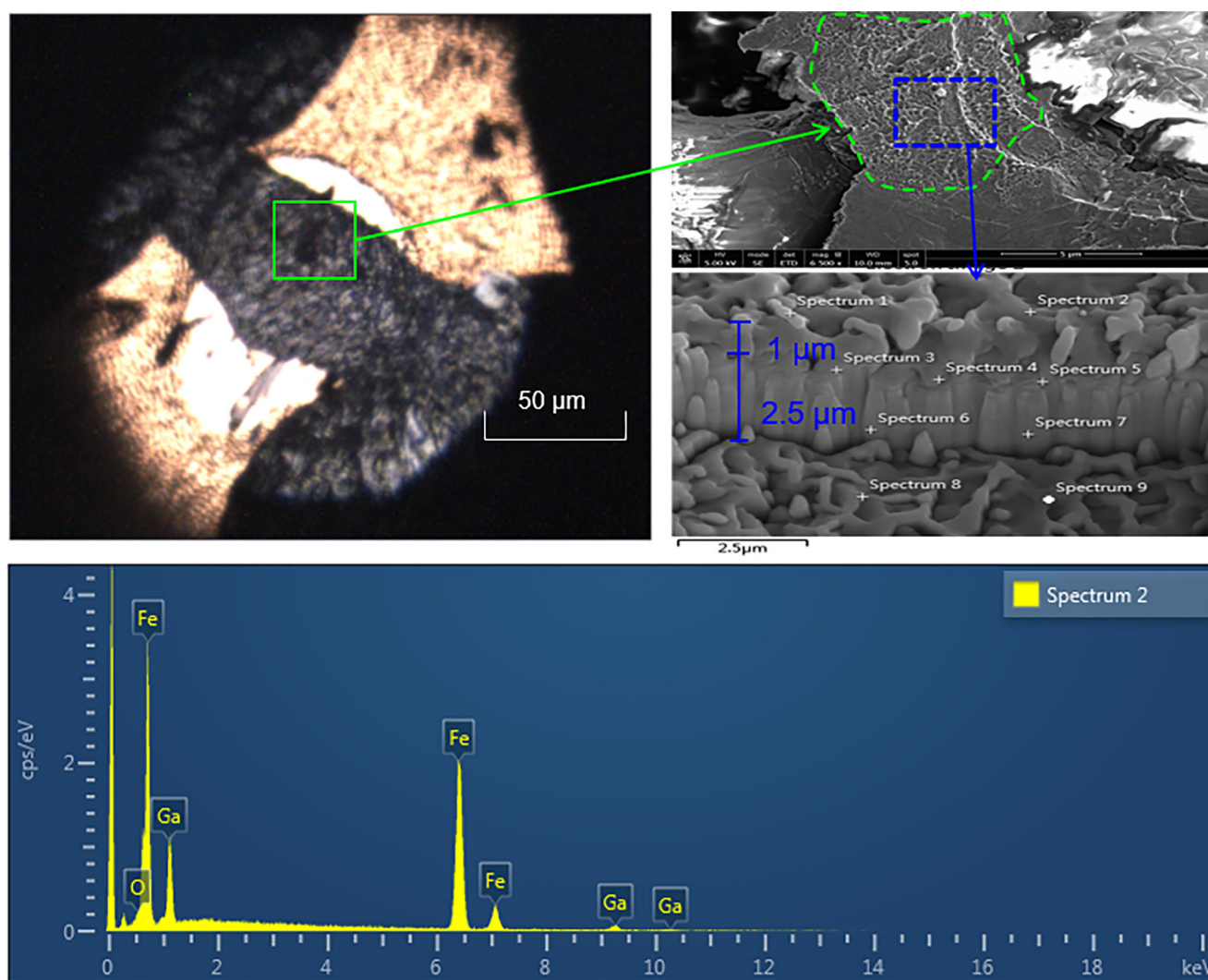


Figure 2. SEM of iron sample recovered from $P_0 = 48$ GPa and 2900 K. Focused ion beam (Ga source) was used to mill a ~ 3.5 - μm hole. The thickness of melted area was about $1.0\ \mu\text{m}$, featured with a flocculent surface. The unmelted area was characterized by pin-like grains. EDS was used to analyze the chemical composition of the quench sample. SiO_2 was not observed within the iron sample.

noting that estimation of sensitivity by 1–2 vol.% should be the upper bound, because the melting area in Figure 2 was heated for three cycles.

3.2. Phase Boundaries of Iron at High Pressure

The slow-fast recrystallization of the hcp iron was first reported by Anzellini et al. (2013). Interestingly, it could be clearly identified in the T - R/R_0 relation (Figure S3 in Supporting Information S1). It was observed in the heating cycles at 56.5 GPa (M2), 68.0 GPa (M5), and 77.5 GPa (M3) (Table S1 in Supporting Information S1). Slope changes were also observed at ~ 2544 and ~ 2700 K for experiments at $P_0 = 116.0$ and 109.0 GPa, respectively. We note that the slope at $P_0 = 97.0$ GPa kept unvarying prior to melting. It might be due to the laser heating spot located at the previously heated area. The kink in the T - R/R_0 relation, which reflected the low-fast recrystallization, may only appear when heating a fresh sample surface. In the field of slow recrystallization, the grain size could be small and the grain boundary had a significant influence on electron flow. By contrast, in the field of fast recrystallization, the grain size became large and the barrier caused by grain boundary would be reduced (Figure 2). During the second heating cycle at the same position, the grain size might not increase evidently, so as to have a negligible impact on the T - R/R_0 relation.

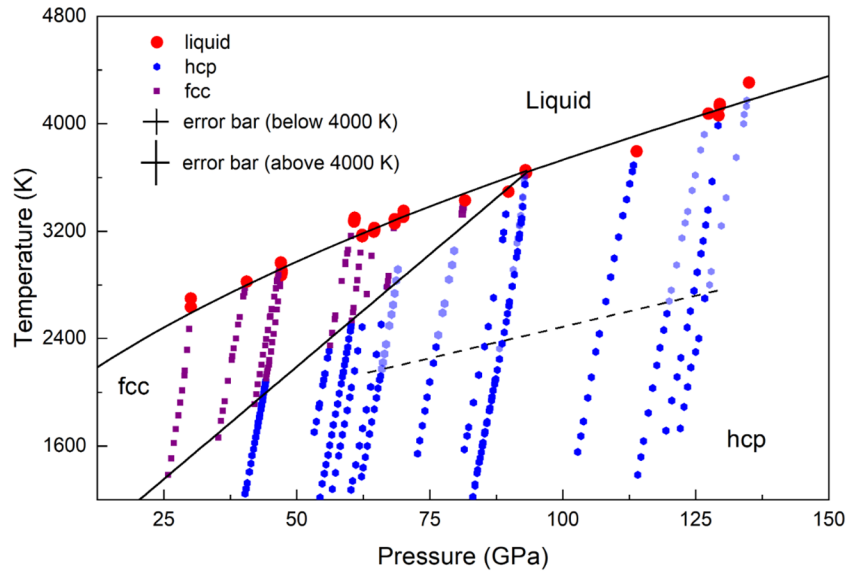


Figure 3. Pressure-temperature conditions at which electrical resistance measurements on iron have been collected. Solid curves represent the phase boundaries between fcc, hcp, and liquid iron. The dashed curve is the slow-fast recrystallization boundary. The temperature was calculated from the radiation spectra in the wavelength range of 600–750 nm. Hexagons (light blue) represent fast recrystallization.

In this study, the boundary of the low-fast recrystallization should be placed at 2140–2770 K at P_T ranging from 66 to 128 GPa (Figure 3).

The solid-solid phase transition was determined by both T - R/R_0 and T -Power relations, while the solid-liquid phase transition by the aforementioned four criteria. The pressure and temperature conditions at which the electrical resistance has been collected are illustrated in Figure 3. The eight experiments ($P_0 = 20$ –56 GPa) were conducted to constrain the hcp-fcc phase boundary of iron. The hcp-fcc phase transition boundary is located at 1362–2780 K in the pressure range of $P_T = 25$ –67 GPa, which could be described by $T = 513(80) + 33.5(16)P_T$ (T in the unit of K and P_T in the unit of GPa).

The melting curve of fcc-Fe was delimited by using a total of 12 data points in this study (Figure 3). The T_m values of fcc-Fe range from 2640 to 3646 K at $P_T = 30$ –93 GPa. We modeled the melting curve of fcc-Fe by an empirical Simon-Glatzel equation (Simon & Glatzel, 1929):

$$T_m = T_{m0} \left(\frac{P_m - P_{m0}}{a} + 1 \right)^{1/c} \quad (1)$$

where a and c are the two composition-dependent constants, while the bcc-fcc-liquid triple point of iron at 5.2 GPa and 1991 K was anchored as the reference point (P_{m0} , T_{m0}) for fitting the melting curve of fcc-Fe (Swartzendruber, 1982). The parameters of $a = 32.27(895)$ and $c = 2.17(36)$ were derived with the least-squares fitting method applied. In this study, the melting curve of fcc-Fe intersects the fcc-hcp phase transition boundary at 93.2 GPa and 3641 K, defining the fcc-hcp-liquid triple point of iron. On the other hand, the melting curve of hcp-Fe was less well constrained at 94–135 GPa with the five melting data points of hcp iron obtained. Alternatively, the melting curve of hcp-Fe was linearly fitted in this narrow pressure range, with the T_m values increasing from 3715(150) K at $P_T = 94$ GPa to 4306(300) K at $P_T = 135$ GPa.

4. Discussion

Large deviations exist in the previous static experiments on the melting curves of iron (Figure 4). Boehler (1993) presented the lowest melting curve with a melting criterion of fluid flow. The low melting curve has been continuously reported by their group using a good number of criteria, such as fast changes of position and intensity of diffraction pattern, diffuse scattering ring in XRD, X-ray absorption spectroscopy,

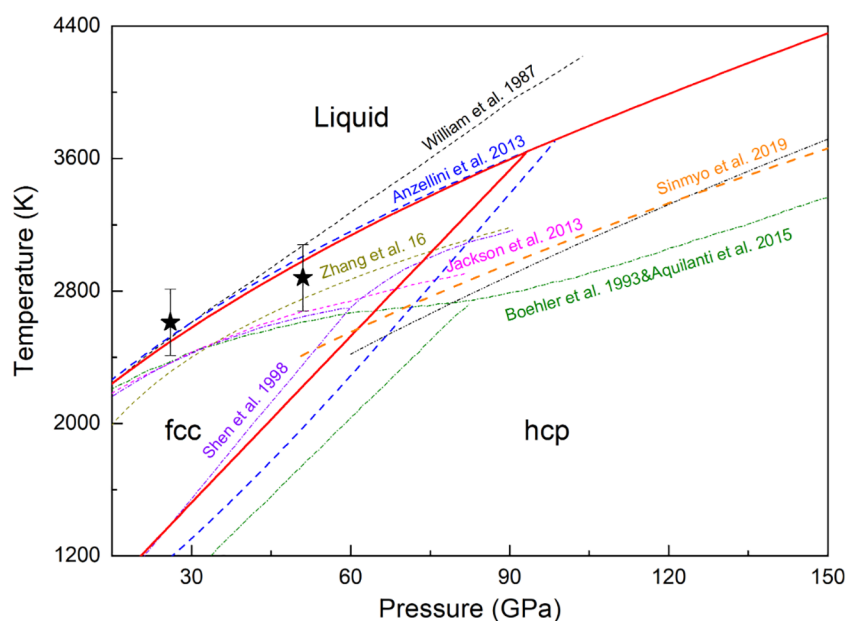


Figure 4. The melting curves of iron obtained in this work and previous studies up to 150 GPa. The solid curve (red) represents the fitted melting curve of iron from this study. Star symbols represent the results from Ohta et al. (2016). The melting curves of hcp-Fe in the current study (red curve) and Anzellini et al. (2013) (blue-dashed curve) are overlapped with each other.

and resistance jump (Aquilanti et al., 2015; Basu et al., 2020; Boehler et al., 2008). On the contrary, the two highest melting curves of iron were proposed by Anzellini et al. (2013) and Williams et al. (1987), with quenched texture and diffuse scattering ring in XRD used as the primary melting criteria, respectively. The intermediate melting curves of iron were reported by using a series of methods, such as the disappearance of X-ray diffraction peaks (Shen et al., 1998) and synchrotron Mössbauer spectroscopy (Jackson et al., 2013; Zhang et al., 2016). The T_m discrepancy of iron at 100 GPa is as large as 1200 K among those studies. In particular, compared to Boehler (1993), this study and Anzellini et al. (2013) reported the T_m values of hcp iron higher by approximately 1000 K at pressures above 100 GPa.

This study confirms the high melting curve of iron by using electrical resistance jump as the primary melting criterion. Our electrical results are consistent with the electrical conductivity measurements of iron at high-pressure and high-temperature conditions by Ohta et al. (2016). They found electrical resistivity jumps at (26 GPa, 2580 K) and (51 GPa, 2900 K), respectively (Figure 4). Our melting curve of fcc-Fe is also in good agreement with Williams et al. (1987) below 60 GPa. In general, the melting curve of iron by this study is well matched with that by Anzellini et al. (2013), although their fcc-hcp-liquid triple point of iron is relatively high at 98.5 GPa and 3712 K. Furthermore, the slow-fast recrystallization boundary was determined by the appearance or disappearance of single-crystal diffraction spots (Anzellini et al., 2013); it is about 500 K higher with respect to that reflected by our resistance discontinuity. Interestingly, it is worth pointing out that the low melting curve by Boehler (1993) is in good agreement with the slow-fast recrystallization boundary of iron reported by Anzellini et al. (2013). In this study, the slow-fast recrystallization boundary of iron is at relatively low temperatures approximately from 2100 K at 60 GPa to 2800 K at 130 GPa. The low boundary may be attributed to the grain size of starting materials as well as that electrical resistance is more sensitive to identify changes in grain boundaries and sizes of the sample upon laser heating at high pressure.

The large variations of melting temperatures of iron among experimental measurements were suggested to be attributed to the melting criteria, oxidation, and/or carbon contamination of the sample (Hirose et al., 2013; Morard et al., 2018). We summarized the melting criteria and pressure media used in the previous studies (Table S2 in Supporting Information S1). The 9 melting criteria were employed to determine the melting of iron at high pressure. Resistance (or voltage) jump in DACs has been used by Basu et al. (2020),

Sinmyo et al. (2019), and this study. In particular, these studies present different T_m values of iron at 2800, 3100, and 3700 K, respectively, at ~ 100 GPa. The melting temperature of iron might be assigned to the resistance discontinuity caused by the sample deformation prior to melting in Basu et al. (2020). Similarly, the discrepancy in the T_m values of iron is as large as 900 K at 100 GPa, which was determined by the same melting criterion besides resistance jump in different studies (e.g., fluid flow, quenched texture, diffuse scattering in the XRD, synchrotron Mössbauer spectroscopy, or X-ray absorption spectroscopy). These results suggest that melting criteria may be not responsible for the large variations of measured melting temperature. On the other hand, the high T_m is less likely due to the iron strip oxidized during sample preparation and/or contaminated by the SiO_2 pressure medium or Fe_3C from the chemical reaction between the sample and diamond anvil, since those materials tend to reduce the melting point of iron at high pressure (Figure 2 and Figure S2 in Supporting Information S1). Likewise, sample oxidation could be excluded based on SEM-EDS measurements on the recovered samples by this study, Basu et al. (2020), Jackson et al. (2013), and Sinmyo et al. (2019).

Meanwhile, a variety of pressure-transmitting media have been employed in the high-pressure and high temperature-experiments, such as oxides (SiO_2 , Al_2O_3 , and MgO), halides (KCl and NaCl), and noble gases (Ar and Xe). Thus far, KCl and Al_2O_3 were most extensively used. With the use of KCl or Al_2O_3 pressure medium, the measured T_m values of iron were reported in a wide range of 2800–3700 and 2800–4100 K, respectively, at 100 GPa when the same melting criterion is applied. That is, the pressure medium may have negligible effects on determining the melting temperature, if the pressure-transmitting medium had been well desiccated and vacuumed with avoiding moisture contamination during sample preparation and compression.

Melting criteria and sample oxidation shall not be the primary factors leading to the large variations in the measured T_m values of iron among static compression experiments. Therefore, other factors shall be taken into account including high-temperature measurements. We note that optical lens can cause chromatic aberrations of the radiation spectra in a refractive optical system that has a significant impact for temperature determination (Walter & Koga, 2004). As the refractive index of a lens is highly wavelength dependent, it would introduce chromatic aberrations in transmitted light. The chromatic aberrations were clearly observed in two typical spectra, in which temperature values were derived with the fitting of different wavelength ranges (Figure S3 in Supporting Information S1). The three wavelength ranges of 600–750 nm, 600–800 nm, and 650–800 nm were tested. We found that spectrum_1 resulted in the calculated temperatures values of 4783, 5006, and 5427 K, corresponding to the three fitting ranges. Similarly, the fitted temperature values of 3728, 3878, and 4090 K for spectrum_2. Intriguingly, the temperature difference can reach as large as about 10% only with considering chromatic aberrations to temperature measurements.

We chose the wavelength range of 600–750 nm to calculate the temperature based on the following two reasons. First, the radiation spectra were calibrated at 2993 K by a standard tungsten lamp and the temperature difference was less than 100 K in the fitted temperatures with the aforementioned three wavelength ranges. Second, we measured the melting temperature of a refractory metal, rhenium (Re), and found that the temperature fitted in the wavelength range of 600–750 nm appeared more reasonable at 50–60 GPa and above (Figures S4–S5 in Supporting Information S1) (Yang et al., 2012). We noticed that the temperature value calculated from the wavelength range of 600–750 nm is less than that from the other two ranges. That is, the temperature calculated between 600 and 750 nm represents the lower bound of temperature measurements in this study. In addition, when the temperature is below 3000 K, the calculated T_m values are hardly affected by chromatic aberrations. Hence, the melting curve of iron can be well constrained without considering chromatic aberrations below 50–55 GPa in this study. However, at 135 GPa, the temperature difference reached 800–900 K due to chromatic aberrations. It indicates that with increasing temperature and pressure, chromatic aberrations become more severe and the increasing temperature difference must be taken into account above 4,000–7000 K in the previous studies.

5. Conclusions

We measured the melting curve of iron at high pressure using resistance jump as a melting criterion in laser-heated DACs, coupled with the other three melting criteria such as the temperature-laser power relation, quench texture, and fluid flow. Our results suggest that the large variations in the melting curve of iron at high pressure are not principally caused by different melting criteria, whereas the effects of chromatic aberrations on temperature measurements shall be included. Furthermore, electrical resistance is sensitive to the incipient melting and changes in grain boundaries and sizes upon heating at high pressure and thus it could be capable of detecting a few percent of molten iron and the onset of the slow-fast recrystallization transition boundary. This work confirms a high melting curve of iron up to 135 GPa, consistent with the fast X-ray diffraction study by Anzellini et al. (2013) and the latest shock experiments by Li et al. (2020). The high melting curve of iron has many long-term implications for the interior structure and thermal evolution of terrestrial planets, the four innermost planets in the solar system. It is conceivable that the higher temperature the liquid iron core has in the early stage, the warmer temperature the present interiors of these planets have (Jackson et al., 2013). Meanwhile, the high melting curve of iron suggests the presence of partial melting in the core-mantle boundary of the Earth due to a high and steep geothermal gradient and a high heat flux across this region (Anzellini et al., 2013).

Data Availability Statement

Data sets for the experimental pressure-temperature conditions are available at the link <https://zenodo.org/record/5219772> (DOI: 10.5281/zenodo.5219772). The data in Table S2 in Supporting Information S1 are available in Anzellini et al. (2013), Aquilanti et al. (2015), Basu et al. (2020), Boehler (1993), Boehler et al. (2008), Jackson et al. (2013), Morard et al. (2018), Shen et al. (1998), Sinmyo et al. (2019), Williams et al. (1987), and Zhang et al. (2016).

Acknowledgments

We thank Dr. Sudeshna Samanta for technical assistance. This work is supported by the National Natural Science Foundation of China (grant no. 42072052 and 42074098) and the B-type Strategic Priority Research Program of Chinese Academy of Sciences (grant no. XDB41000000). M.H. is partially supported by the National Science Foundation (NSF grant no. EAR-1847707).

References

- Alfè, D., Gillan, M. J., & Price, G. D. (2002). Composition and temperature of the Earth's core constrained by combining ab initio calculations and seismic data. *Earth and Planetary Science Letters*, 195(1–2), 91–98. [https://doi.org/10.1016/S0012-821X\(01\)00568-4](https://doi.org/10.1016/S0012-821X(01)00568-4)
- Anzellini, S., Dewaele, A., Mezouar, M., Loubeyre, P., & Morard, G. (2013). Melting of iron at Earth's inner core boundary based on fast X-ray diffraction. *Science*, 340(6131), 464–466. <https://doi.org/10.1126/science.1233514>
- Aquilanti, G., Trapananti, A., Karandikar, A., Kantor, I., Marini, C., Mathon, O., et al. (2015). Melting of iron determined by X-ray absorption spectroscopy to 100 GPa. *Proceedings of the National Academy of Sciences of the United States of America*, 112(39), 12042–12045. <https://doi.org/10.1073/pnas.1502363112>
- Basu, A., Field, M. R., McCulloch, D. G., & Boehler, R. (2020). New measurement of melting and thermal conductivity of iron close to outer core conditions. *Geoscience Frontiers*, 11(2), 565–568. <https://doi.org/10.1016/j.gsf.2019.06.007>
- Boehler, R. (1986). The phase diagram of iron to 430 kbar. *Geophysical Research Letters*, 13(11), 1153–1156. <https://doi.org/10.1029/gl013i011p01153>
- Boehler, R. (1993). Temperatures in the Earth's core from melting-point measurements of iron at high static pressures. *Nature*, 363(6429), 534–536. <https://doi.org/10.1038/363534a0>
- Boehler, R., Santamaría-Pérez, D., Errandonea, D., & Mezouar, M. (2008). Melting, density, and anisotropy of iron at core conditions: New x-ray measurements to 150 GPa. *Journal of Physics: Conference Series*, 121(2), 022018. <https://doi.org/10.1088/1742-6596/121/2/022018>
- Brown, J. M., & McQueen, R. G. (1986). Phase transitions, Grüneisen parameter, and elasticity for shocked iron between 77 GPa and 400 GPa. *Journal of Geophysical Research*, 91(B7), 7485–7494. <https://doi.org/10.1029/jb091i07p07485>
- Deng, L., Seagle, C., Fei, Y., & Shahar, A. (2013). High pressure and temperature electrical resistivity of iron and implications for planetary cores. *Geophysical Research Letters*, 40(1), 33–37. <https://doi.org/10.1029/2012gl054347>
- Dorogokupets, P., Dymshits, A., Litasov, K., & Sokolova, T. (2017). Thermodynamics and equations of state of iron to 350 GPa and 6000 K. *Scientific Reports*, 7, 41863. <https://doi.org/10.1038/srep41863>
- Fei, Y., Murphy, C., Shibazaki, Y., Shahar, A., & Huang, H. (2016). Thermal equation of state of hcp-iron: Constraint on the density deficit of Earth's solid inner core. *Geophysical Research Letters*, 43, 6837–6843. <https://doi.org/10.1002/2016gl069456>
- Hirose, K., Labrosse, S., & Hernlund, J. (2013). Composition and state of the core. *Annual Review of Earth and Planetary Sciences*, 41, 657–691. <https://doi.org/10.1146/annurev-earth-050212-124007>
- Hou, M. (2016). *Toward a consensus on melting of iron at high pressure*. AGUFM, 2016, MR33B-2684.
- Jackson, J. M., Sturhahn, W., Lerche, M., Zhao, J., Toellner, T. S., Alp, E. E., et al. (2013). Melting of compressed iron by monitoring atomic dynamics. *Earth and Planetary Science Letters*, 362, 143–150. <https://doi.org/10.1016/j.epsl.2012.11.048>
- Li, J., Wu, Q., Li, J., Xue, T., Tan, Y., Zhou, X., et al. (2020). Shock melting curve of iron: A consensus on the temperature at the Earth's inner core boundary. *Geophysical Research Letters*, 47(15), e2020GL087758. <https://doi.org/10.1029/2020gl087758>
- Liu, J., Lin, J. F., Prakapenka, V. B., Prescher, C., & Yoshino, T. (2016). Phase relations of Fe₃C and Fe₇C₃ up to 185 GPa and 5200 K: Implication for the stability of iron carbide in the Earth's core. *Geophysical Research Letters*, 43(24), 12415–12422. <https://doi.org/10.1002/2016gl071353>
- Liu, L. G., & Bassett, W. A. (1975). The melting of iron up to 200 kbar. *Journal of Geophysical Research*, 80(26), 3777–3782. <https://doi.org/10.1029/jb080i026p03777>

- Mao, H., Bell, P., & Hadidiacos, C. (1987). Experimental phase relations of iron to 360 kbar, 1400 C, determined in an internally heated diamond-anvil apparatus. In *High-pressure Research in mineral physics* (pp. 135–138). Terra Scientific/AGU. <https://doi.org/10.1029/gm039p0135>
- Morard, G., Andrault, D., Antonangeli, D., Nakajima, Y., Auzende, A. L., Boulard, E., et al. (2017). Fe–FeO and Fe–Fe₃C melting relations at Earth's core–mantle boundary conditions: Implications for a volatile-rich or oxygen-rich core. *Earth and Planetary Science Letters*, 473, 94–103. <https://doi.org/10.1016/j.epsl.2017.05.024>
- Morard, G., Andrault, D., Guignot, N., Sanloup, C., Mezouar, M., Petitgirard, S., & Fiquet, G. (2008). In situ determination of Fe–Fe₃S phase diagram and liquid structural properties up to 65 GPa. *Earth and Planetary Science Letters*, 272(3–4), 620–626. <https://doi.org/10.1016/j.epsl.2008.05.028>
- Morard, G., Boccato, S., Rosa, A. D., Anzellini, S., Miozzi, F., Henry, L., et al. (2018). Solving controversies on the iron phase diagram under high pressure. *Geophysical Research Letters*, 45(20), 11074–11082. <https://doi.org/10.1029/2018gl079950>
- Murphy, C. A., Jackson, J. M., Sturhahn, W., & Chen, B. (2011). Melting and thermal pressure of hcp-Fe from the phonon density of states. *Physics of the Earth and Planetary Interiors*, 188(1–2), 114–120. <https://doi.org/10.1016/j.pepi.2011.07.001>
- Nguyen, J. H., & Holmes, N. C. (2004). Melting of iron at the physical conditions of the Earth's core. *Nature*, 427(6972), 339–342. <https://doi.org/10.1038/nature02248>
- Ohta, K., Kuwayama, Y., Hirose, K., Shimizu, K., & Ohishi, Y. (2016). Experimental determination of the electrical resistivity of iron at Earth's core conditions. *Nature*, 534(7605), 95–98. <https://doi.org/10.1038/nature17957>
- Shen, G., Mao, H. K., Hemley, R. J., Duffy, T. S., & Rivers, M. L. (1998). Melting and crystal structure of iron at high pressures and temperatures. *Geophysical Research Letters*, 25(3), 373–376. <https://doi.org/10.1029/97gl03776>
- Silber, R. E., Secco, R. A., Yong, W., & Littleton, J. (2018). Electrical resistivity of liquid Fe to 12 GPa: Implications for heat flow in cores of terrestrial bodies. *Scientific Reports*, 8(1), 10758. <https://doi.org/10.1038/s41598-018-28921-w>
- Simon, F., & Glatzel, G. (1929). Remarks on fusion pressure curve. *Zeitschrift für Anorganische und Allgemeine Chemie*, 178(1), 309–316. <https://doi.org/10.1002/zaac.19291780123>
- Sinmyo, R., Hirose, K., & Ohishi, Y. (2019). Melting curve of iron to 290 GPa determined in a resistance-heated diamond-anvil cell. *Earth and Planetary Science Letters*, 510, 45–52. <https://doi.org/10.1016/j.epsl.2019.01.006>
- Swartzendruber, L. (1982). The Fe (iron) system. *Bulletin of Alloy Phase Diagrams*, 3(2), 161–165. <https://doi.org/10.1007/bf02892374>
- Turneure, S., Sharma, S., & Gupta, Y. M. (2020). Crystal structure and melting of Fe shock compressed to 273 GPa: In situ X-Ray diffraction. *Physical Review Letters*, 125(21), 215702. <https://doi.org/10.1103/physrevlett.125.215702>
- Vočadlo, L., Alfè, D., Gillan, M. J., & Price, G. D. (2003). The properties of iron under core conditions from first principles calculations. *Physics of the Earth and Planetary Interiors*, 140(1–3), 101–125.
- Vočadlo, L., Brodholt, J., Alfè, D., Price, G. D., & Gillan, M. J. (1999). The structure of iron under the conditions of the Earth's inner core. *Geophysical Research Letters*, 26(9), 1231–1234.
- Walter, M. J., & Koga, K. T. (2004). The effects of chromatic dispersion on temperature measurement in the laser-heated diamond anvil cell. *Physics of the Earth and Planetary Interiors*, 143, 541–558. <https://doi.org/10.1016/j.pepi.2003.09.019>
- Williams, Q., Jeanloz, R., Bass, J., Svendsen, B., & Ahrens, T. J. (1987). The melting curve of iron to 250 gigapascals: A constraint on the temperature at Earth's center. *Science*, 236(4798), 181–182. <https://doi.org/10.1126/science.236.4798.181>
- Williams, Q., Knittle, E., & Jeanloz, R. (1991). The high-pressure melting curve of iron: A technical discussion. *Journal of Geophysical Research*, 96(B2), 2171–2184. <https://doi.org/10.1029/90jb01999>
- Yang, L., Karandikar, A., & Boehler, R. (2012). Flash heating in the diamond cell: Melting curve of rhenium. *Review of Scientific Instruments*, 83(6), 063905. <https://doi.org/10.1063/1.4730595>
- Yong, W., Secco, R. A., Littleton, J., & Silber, R. E. (2019). The iron invariance: Implications for thermal convection in Earth's core. *Geophysical Research Letters*, 46(20), 11065–11070. <https://doi.org/10.1029/2019gl084485>
- Yoo, C. S., Holmes, N. C., Ross, M., Webb, D. J., & Pike, C. (1993). Shock temperatures and melting of iron at Earth core conditions. *Physical Review Letters*, 70(25), 3931–3934. <https://doi.org/10.1103/physrevlett.70.3931>
- Zhang, D., Jackson, J. M., Zhao, J., Sturhahn, W., Alp, E. E., Hu, M. Y., et al. (2016). Temperature of Earth's core constrained from melting of Fe and Fe 0.9 Ni 0.1 at high pressures. *Earth and Planetary Science Letters*, 447, 72–83. <https://doi.org/10.1016/j.epsl.2016.04.026>
- Zhang, Y., Hou, M., Driscoll, P., Salke, N. P., Liu, J., Greenberg, E., et al. (2021). Transport properties of Fe–Ni–Si alloys at Earth's core conditions: Insight into the viability of thermal and compositional convection. *Earth and Planetary Science Letters*, 553, 116614. <https://doi.org/10.1016/j.epsl.2020.116614>
- Zhang, Y., Hou, M., Liu, G., Zhang, C., Prakapenka, V. B., Greenberg, E., et al. (2020). Reconciliation of experiments and theory on transport properties of iron and the geodynamo. *Physical Review Letters*, 125(7), 078501. <https://doi.org/10.1103/physrevlett.125.078501>